Journal of Superconductivity and Novel Magnetism (2018) 31:3217–3222
https://doi.org/10.1007/s10948-018-4584-0

ORIGINAL PAPER

Influence of Thickness on the Structural, Optical and Magnetic Properties of Bismuth Ferrite Thin Films

Hamed Maleki[1] · Shahrzad Falahatnezhad[1] · Majid Taraz[1]

Received: 11 December 2017 / Accepted: 22 January 2018 / Published online: 1 February 2018

Abstract
In this paper, the effect of thickness on the structural, optical, and magnetic properties of the $BiFeO_3$ (BFO) thin films formed on a glass substrate by the chemical solution deposition has been studied. The sol-gel method combined by the spin-coating technique is used to fabricate BFO thin films. The XRD analysis indicated that BFO thin films had a rhombohedral perovskite structure. Polycrystallinity, smooth and compact surface morphology, and uniform size distribution, as well as average thickness of layers, were observed in FESEM images. UV-vis spectra showed that the absorption coefficient and energy bandgap increased by increasing the thickness of films. VSM measurements indicated that the thin films showed a behavior between weak ferromagnetic and anti-ferromagnetism for all samples.

Keywords Sol-gel process · Multiferroics · Spin coating technique · Bismuth ferrite · Thin film

1 Introduction

Discovery of the coexistence of ferroelectricity and magnetism in $BiFeO_3$ (BFO) thin film starts a great interest in the study of multifunctional materials [1, 2]. Multiferroics are labeled as materials that show simultaneously more than two ferroic manners, which are ferromagnetic, ferroelectric, and ferroelastic orders [1–7]. The potential application of these materials is in the information storage, sensors, photocatalysts, photovoltaic cells, and spintronic [8–15]. Bismuth ferrite is the only room temperature multiferroic material ($T_c \sim 1103$ K and $T_N \sim 64$ K) [1, 4] and shows a direct energy bandgap of ~2.2 eV [16]. In addition, bismuth ferrite has a rhombohedrally distorted perovskite structure with the space group R_3C [17].

In the last two decades, $BiFeO_3$ was studied theoretically and experimentally. These studies were focused on bismuth ferrite thin film, ceramics, nanoparticles, and nanorods [18–24]. In recent years, different preparation methods have been successfully developed for fabricating $BiFeO_3$ films such as molecular beam epitaxy (MBE) [25–28], RF-sputtering [29–33], pulsed laser deposition (PLD) [14, 33, 34], chemical vapor deposition (CVD) [35–37], and chemical solution deposition [38–40]. Among these methods, solution-derived $BiFeO_3$ thin films (i.e., sol-gel spin coating) have been implemented as a more practical and more adaptable route for industry. This is due to many potential advantages for deposition of thin films including easy operation and low cost. In addition, high purity, good homogeneity, and lower processing temperature are some of the benefits. However, it has less control over thickness and morphology of products during the procedure.

Here, we study the influence of thickness of thin films on morphological, structural, optical, and magnetic properties of bismuth ferrite thin films. Our experiments were carried out on a series of 135–530-nm-thick $BiFeO_3$ films grown by the sol-gel route combined with the spin coating method.

2 Experimental Method

2.1 Fabrication of BFO Layers

Bismuth nitrate (99%, Sigma), iron nitrate (99%, Merck), 2-methoxyethanol (99.5%, Merck), acetic acid (96%, Merck),

✉ Hamed Maleki
hamed.maleki@uk.ac.ir

[1] Faculty of Physics, Shahid Bahonar University of Kerman, Kerman, Iran

and absolute ethanol (99.9%, Merck) were used in this work. $BiFeO_3$ (BFO) thin films with average thickness of 135 (BFO5), 270 (BFO10), 400 (BFO15), and 530 (BFO20) nm have been fabricated using the sol-gel method combined with the spin coating technique. Suitable stoichiometric amounts of bismuth nitrate and iron nitrate are dissolved in 2-methoxyethanol (2-MOE) [42–44]. The whole preparation process was performed in an air atmosphere at room temperature (RT). In order for the pH value to reach 1.5, acetic acid (as the chelating agent) was added dropwise under constant stirring After stirring at RT for an hour, the temperature was increased to 70 °C. After a few hours, a clear brownish sol was obtained. The sol was kept at RT for 2 h and the deposition process was started. The BFO layer was first spin-coated (at 4000 rpm for 30 s) on the wellcleaned glass substrate, and dried at 110 °C for 10 min. To achieve the desired thickness of samples, the process was repeated 5 (BFO5), 10 (BFO10), 15 (BFO15) and 20 (BFO20) times. According to the cross-section field-emission scanning electron microscopy (FESEM) observations, the thickness of each layer was ∼ 27 nm.

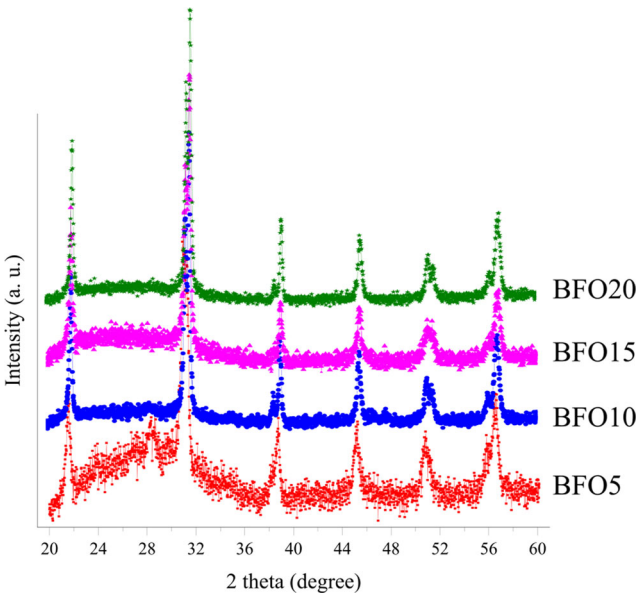

Fig. 1 XRD patterns of $BiFeO_3$ thin films with different thicknesses

2.2 Characterization

The structural properties, average particle size, and phase purity of BFO thin films were characterized by x-ray diffraction measurements using a powder diffractometer (Philips) with Cu-Kα radiation ($\lambda = 1.5406$ Å). The morphology and size of products as well as the thickness of films were determined from the image of BFO thin films using a MIRA3 TESCAN-XMU field-emission scanning electron microscope (FE-SEM). To study the optical properties of samples, room temperature UV-vis diffuse reflectance spectra were measured using a Lambda900 spectrometer. For the magnetic behavior of thin films, the hysteresis loops of BFO films were measured up to 20 KG by using a vibrating sample magnetometer (VSM- Lake Shore model 7410, SAIF).

3 Results

3.1 Structure of $BiFeO_3$ Thin Films

The structural properties of BFO thin films and particle size are investigated by using xray diffraction (XRD) patterns (Fig. 1). Analysis of XRD patterns shows that products have a perovskite structure with a random orientation. For the BFO5 sample, an amorphous behavior and secondary phases with low peak intensity is observed. However, for BFO10, BFO15, and BFO20, no secondary phases were found. Furthermore, the average full width at half maxima (FWHM) value increased as the thickness of the layer increased. The crystallite size of BFO nanocrystals was calculated from Scherrer's equation $D = \frac{K\lambda}{\beta \cos\theta}$, where β is the FWHM, K is the shape factor ∼0.89, λ is the wavelength of the X-ray source, and θ is the Bragg angle of each peak [45]. The average crystallite grain of BFO thin films was calculated to be 28, 38, 47, and 53 nm for BFO5, BFO10, BFO15, and BFO20 respectively.

3.2 FESEM and Morphology Studies

Figure 2a–c shows the images obtained from the field emitted scanning electron microscopy (FESEM) for BFO10 at different magnifications. In these images, uniform grain structure is evident and the average grain size of 35–40 nm is obtained. Some pores were also observed in the sample. The FESEM image for the cross section of the BFO10 thin film is also presented in Fig. 2d. The image shows a sharp interface, flat surface, and the average thickness of 273.92 nm for BFO10.

3.3 Optical Properties of BFO Thin Films

The UV-vis absorption spectra of bismuth ferrite thin films are shown in Fig. 3. For all samples, the absorbance starts before the visible region. The absorption coefficient (α) is increased by increasing the thickness of the BFO layer. Also, there is a shoulder centered at ∼380 nm which could correspond to dipole-allowed charge transfer excitations [46, 47].

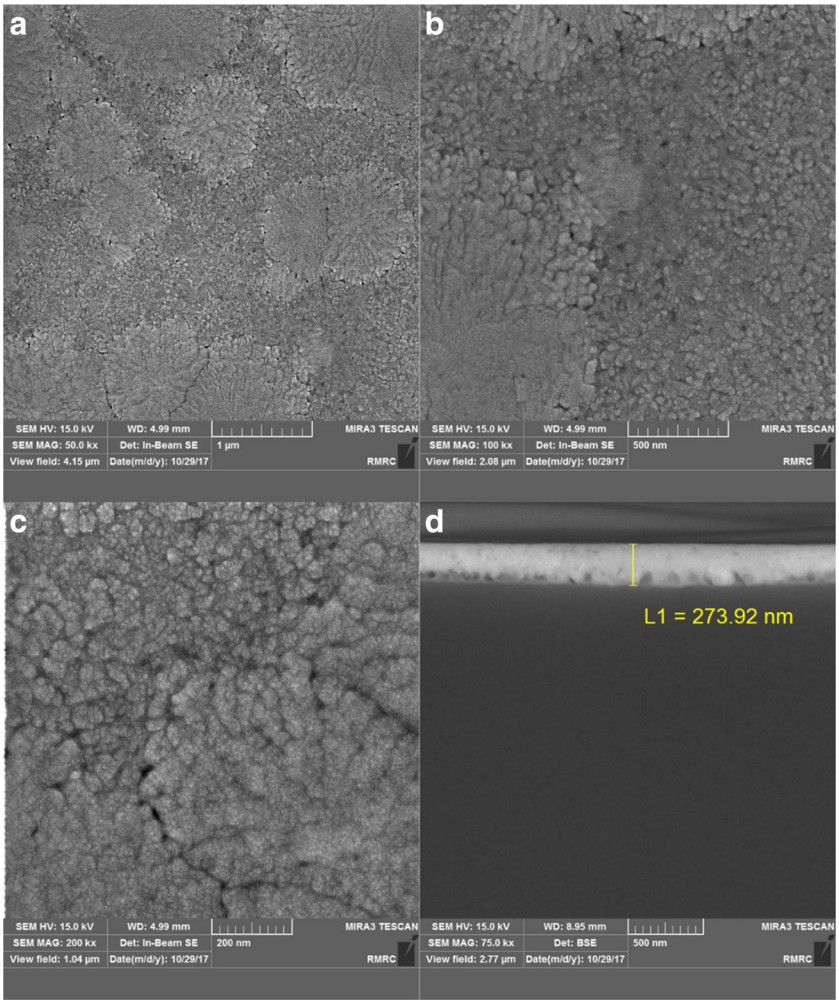

Fig. 2 **a**–**c** FESEM image of BFO10 at different magnifications, **d** cross-sectional FESEM image of the BFO10 thin film on glass substrate

Bismuth ferrite has a direct energy bandgap at RT [9]. The bandgap energy of whole thin films was calculated using Tauc's equation [48] $(\alpha h\nu)^2 = K(h\nu - E_g)$, where K is a constant and $h\nu$ is the photon energy. The curves of $(\alpha h\nu)^2$ versus $h\nu$ for BFO5, BFO10, BFO15, and BFO20 are illustrated in Fig. 4. The optical bandgap was estimated by the linear extrapolation of $(\alpha h\nu)^2$ versus $h\nu$. The calculated bandgap energies of BFO thin films were 1.63 eV for BFO5, 2.35 eV for BFO10, 2.53 eV for BFO15, and 2.82 eV for BFO20 samples. Hence, by increasing the thickness of the BFO layer, the bandgap is increased.

3.4 Hysteresis Loops and Magnetic Properties

Figure 5 shows the magnetic hysteresis loops for bismuth ferrite thin films with different thicknesses at RT. A completely saturated magnetization was not observed for thin films at a maximum applied magnetic field of 20 KG. All samples show a combination of weak ferromagnetic and antiferromagnetic behavior. According to the literature, in bismuth ferrite, the iron ions (Fe^{3+}) have a strong relationship with magnetization and these ions are responsible for magnetic properties of this matter. Surrounding each (Fe^{3+}) ion

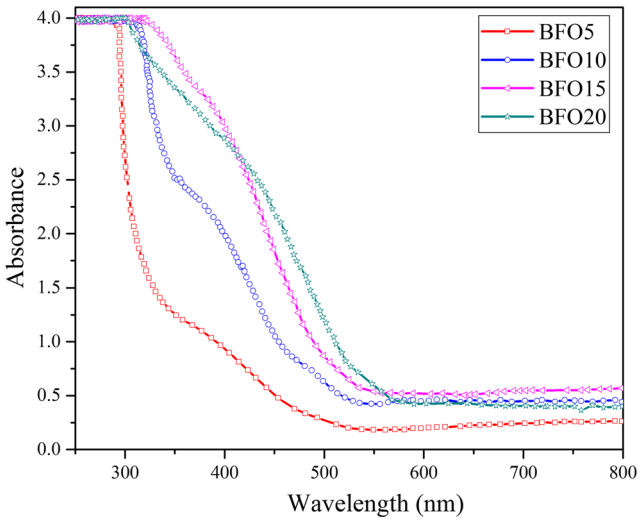

Fig. 3 UV-vis spectrum of $BiFeO_3$ thin films with different thicknesses

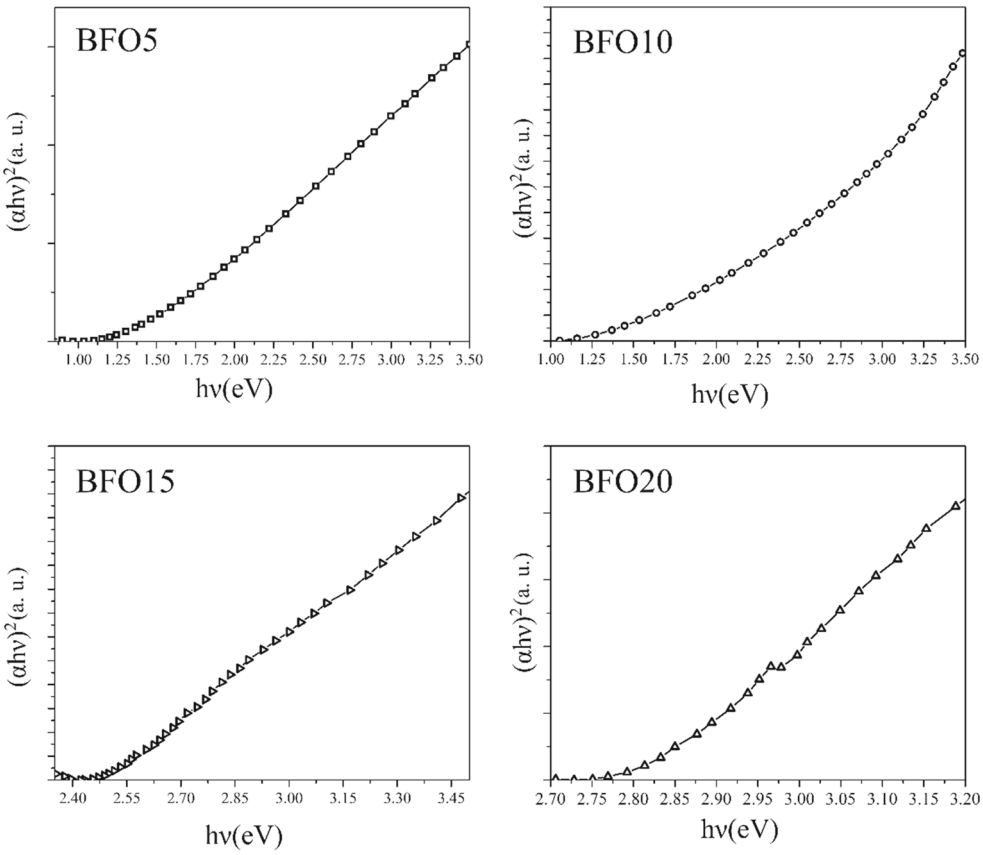

Fig. 4 $(\alpha h\nu)^2$ versus $h\nu$ plots of BFO5, BFO10, BFO15, and BFO20

with a certain spin, there are six other ions with nonparallel spins. These spins are not completely nonparallel; however, they are organized in a spiral manner with a period of 62 nm, which leads to a magnetization value of zero. Breaking the spiral organization of the spin is due to nanoparticle size reduction to less than 62 nm and the rise of uncompensated spins on the surface of nanocrystals (because of a rise of area relative to volume). This can be a justification for the increase in magnetic properties and the decline in ferromagnetic properties of bismuth ferrite [9].

By increasing the thickness of layers, saturated magnetization (M_s) decreases. On the other hand, remanent magnetization (M_r) and coercive force (H_c) increase. Table 1 shows the information from magnetic characterization tests for the prepared BFO thin films with different thicknesses.

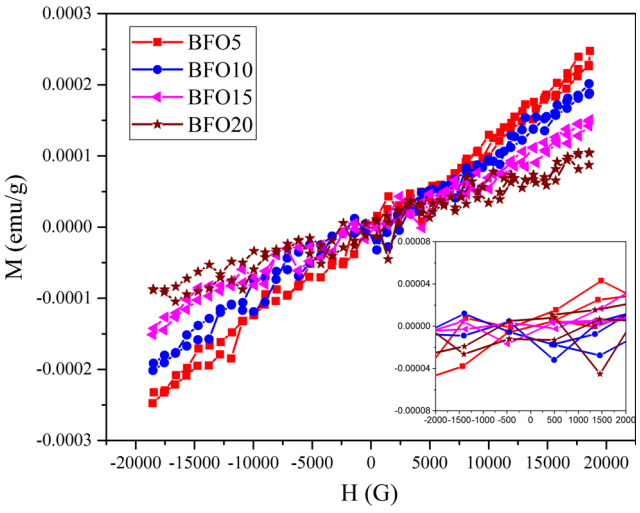

Fig. 5 Room temperature magnetic hysteresis loops of $BiFeO_3$ thin films with different thicknesses

Table 1 Information from magnetic characterization for BFO thin films

Sample	$M_s \times 10^{-6}$(emu/g)	$M_r \times 10^{-6}$(emu/g)	H_c(G)
BFO5	247.6	3.3	92.4
BFO10	201.5	3.6	38.6
BFO15	151.2	9.5	717.2
BFO20	104.7	895.2	1643.5

4 Conclusions

In summary, $BiFeO_3$ thin films with different thicknesses were successfully fabricated on glass substrate by the sol-gel spin coating process. The influence of thickness of films on the structural, optical, and magnetic properties of the films was studied. X-ray diffraction showed that all thin films had a single $BiFeO_3$ phase with rhombohedral perovskite structure and space group R_3C. The degree of crystallinity and crystallite size increased with the increasing of the thickness of the BFO layer. The FESEM micrographs revealed the formation of particles with average size of 35–40 nm for the BFO10 sample. The thickness of each coated layer is obtained ∼27 nm. The UV-vis absorption spectra of bismuth ferrite thin films indicated that the energy bandgap increases by the increasing of the thickness of thin films and changes from 1.63 eV for BFO5 to 2.82 eV for BFO20. A mixture of weak ferromagnetic and anti-ferromagnetic behavior is observed for bismuth ferrite thin films. Moreover, an increasing in H_c is obtained by increasing the thickness of the BFO layer. Considering the results from VSM, one can see that as the thickness of the BFO layer is increased, the saturation magnetizations decrease.

References

1. Wang, J., Neaton, J.B., Zheng, H., Nagarajan, V., Ogale, S.B., Liu, B., Viehland, D., Vaithyanathan, V., Schlom, D.G., Waghmare, U.V., Spaldin, N.A., Rabe, K.M., Wuttig, M., Ramesh, R.: Science **299**, 1719 (2003)
2. Palkar, V.R., John, J., Pinto, R.: Appl. Phys. Lett. **80**, 1628 (2002)
3. Hill, N.A.: J. Chem. Phys. B **104**, 6694 (2000)
4. Eerenstein, W., Mathur, N.D., Scott, J.F.: Nature **442**, 759 (2006)
5. Ramesh, R., Spaldin, N.A.: Nat. Mater. **6**, 21 (2007)
6. Choi, T., Lee, S., Choi, Y.J., Kiryukhin, V., Cheong, S.W.: Science **324**, 63 (2009)
7. Zhang, Q., Sando, D., Nagarajan, V.: J. Mater. Chem. C **4**, 4092 (2016)
8. Dong, S., Liu, J.M., Cheong, S.W., Ren, Z.F.: Adv. Phys. **64**, 519 (2015)
9. Catalan, G., Scott, J.F.: Adv. Mater. **21**, 2463 (2009)
10. Gao, F., Chen, X.Y., Yin, B.K., Dong, S., Ren, Z.F., Yuan, F., Yu, T., Zou, Z.G., Lui, J.M.: Adv. Mater. **19**, 2889 (2007)
11. Scott, J.F.: J. Mat. Chem. **22**, 4567 (2012)
12. Zhao, T., Scholl, A., Zavaliche, F., Lee, K., Barry, M., Doran, A., Cruz, M.P., Chu, Y.H., Ederer, C., Spaldin, N.A., Das, R.R., Kim, D.M., Baek, S.H., Eom, C.B., Ramesh, R.: Nat. Mater. **5**, 823 (2006)
13. Liu, H., Yang, X.: Ferroelectrics **507**, 69 (2017)
14. Pabst, G.W., Martin, L.W., Chu, Y.H., Ramesh, R.: Appl. Phys. Lett. **90**, 072902 (2007)
15. Ramazanoglu, M., Ratcliff, W., Choi, Y.J., Lee, S., Cheong, S.W., Kiryukhin, V.: Phys. Rev. B **83**, 174434 (2011)
16. Xu, X., Lin, Y.H., Li, P., Shu, L., Nan, C.W.: J. Am. Ceram. Soc. **94**, 2296 (2011)
17. Jang, H.W., Baek, S.H., Ortiz, D., Folkman, C.M., Das, R.R., Ramesh, R.: Phys. Rev. Lett. **101**, 107602 (2008)
18. Ederer, C., Spaldin, N.A.: Phys. Rev. B **71**(R), 060401 (2005)
19. Lebeugle, D., Colson, D., Forget, A., Viret, M., Bonville, P., Marucco, J.F., Fusil, S.: Phys. Rev. B **76**, 024116 (2007)
20. Lubk, A., Gemming, S., Spaldin, N.A.: Phys. Rev. B **80**, 104110 (2009)
21. Ravindran, P., Vidya, R., Kjekshus, A., Fjellvag, H., Eriksson, O.: Phys. Rev. B **74**, 224412 (2006)
22. Scott, J.F.: J. Magn. Magn. Mater. **321**, 1689 (2009)
23. Jha, P.K., Jha, P.A., Srivastava, G., Jha, A.K., Kotnala, R.K., Dwivedi, R.K.: J. Magn. Magn. Mater. **349**, 95 (2014)
24. Sun, Y., Sun, Z., Wei, R., Huang, Y., Wang, L., Leng, J., Xiang, P., Lan, M.: J. Magn. Magn. Mater. **449**, 10 (2018)
25. Ihlefeld, J.F., Kumar, A., Gopalan, V., Schlom, D.G., Chen, Y.B., Pan, X.Q., Heeg, T., Schubert, J., Ke, X., Schiffer, P., Orenstein, J., Martin, L.W., Chu, Y.H., Ramesh, R.: Appl. Phys. Lett. **91**, 071922 (2007)
26. Kim, D.H., Aimon, N.M., Sun, X.Y., Kornblum, L., Walker, F.J., Ahn, C.H., Ross, C.A.: Adv. Funct. Mater. **24**, 5889 (2014)
27. Laughlin, R.P., Currie, D.A., Contreras-Guererro, R., Dedigama, A., Priyantha, W., Droopad, R., Theodoropoulou, N., Gao, P., Pan, X.: J. Appl. Phys. **113**, 17D919 (2013)
28. Deepak, N., Carolan, P., Keeney, L., Zhang, P.F., Pemble, M.E., Whatmore, R.W.: Chem. Mater. **27**, 6508 (2015)
29. Aramaki, M., Kariya, K., Yoshimura, T., Murakami, S., Fujimura, N.: Jpn. J. Appl. Phys. **55**, 10TA16 (2016)
30. Ramirez-Camacho, M.C., Sanchez-Valdes, C.F., Gervacio-Arciniega, J.J., Font, R., Ostos, C., Bueno-Baques, D., Curiel, M., Sanchez-Llamazares, J.L., Siqueiros, J.M., Raymond-Herrera, O.: Acta Materialia **128**, 451 (2017)
31. Mori, T.J.A., Mouls, C.L., Morgado, F.F., Schio, P., Cezar, J.C.: J. Appl. Phys. **122**, 124102 (2017)
32. Zheng, R.Y., Gao, X.S., Zhou, Z.H., Wang, J.: J. Appl. Phys. **101**, 054104 (2007)
33. Cho, S., Jang, J.W., Zhang, W., Suwardi, A., Wang, H., Wang, D., MacManus-Driscoll, J.L.: Chem. Mater. **27**, 6635 (2015)
34. Katiyar, R.K., Sharma, Y., Misra, P., Puli, V.S., Sahoo, S., Kumar, A., Scott, J.F., Morell, G., Weiner, B.R., Katiyar, R.S.: Appl. Phys. Lett. **105**, 172904 (2014)
35. Moniz, S.J.A., Quesada-Cabrera, R., Blackman, C.S., Tang, J., Southern, P., Weaver, P.M., Carmalt, C.J.: J. Mater. Chem. A **2**, 2922 (2014)
36. Yang, S.Y., Zavaliche, F., Mohaddes-Ardabili, L., Vaithyanathan, V., Schlom, D.G., Lee, Y.J., Chu, Y.H., Cruz, M.P., Zhan, Q., Zhao, T., Ramesh, R.: Appl. Phys. Lett. **87**, 102903 (2005)
37. Moniz, S.J.A., Blackman, C.S., Southern, P., Weaver, P.M., Tanga, J., Carmalt, C.J.: Nanoscale **7**, 16343 (2015)
38. Naganuma, H., Okamura, S., Appl, J.: J. Appl. Phys. **101**, 09M103 (2007)
39. Dong, G., Tan, G., Luo, Y., Liu, W., Xia, A., Ren, H.: Appl. Surf. Sci. **305**, 55 (2014)
40. Tomczyk, M., Stroppa, D.G., Reaney, I.M., Vilarinho, P.M.: Phys. Chem. Chem. Phys. **19**, 14337 (2017)
41. Zhang, H.R., Kalantari, K., Marincel, D.M., Trolier-McKinstry, S., MacLaren, I., Ramasse, Q.M., Rainforth, W.M., Reaney, I.M.: Thin Solid Films **616**, 767 (2016)
42. Hu, W.W., Chen, Y., Yuan, H.M., Li, G.H., Qiao, Y., Qin, Y.Y., Feng, S.H.: J. Phys. Chem. C **115**, 8869 (2011)
43. Tyholdt, F., Jorgensen, S., Fjellvag, H., Gunnaes, A.E.: J. Mater. Res. **20**, 2127 (2005)
44. Zhang, Q., Valanoor, N., Standard, O.: J. Mater. Chem. C **3**, 582 (2015)

45. Cullity, B.D., Stock, S.R.: Elements of X ray Diffraction. Prentice Hall, Upper Saddle River (2001)
46. Xu, X.S., Brinzari, T.V., Lee, S., Chu, Y.H., Martin, L.W., Kumar, A., McGill, S., Rai, R.C., Ramesh, R., Gopalan, V., Cheong, S.W., Musfeldt, J.L.: Phys. Rev. B **79**, 134425 (2009)
47. Xu, X.S., Ihlefeld, J.F., Lee, J.H., Ezekoye, O.K., Vlahos, E., Ramesh, R., Gopalan, V., Pan, X.Q., Schlom, D.G., Musfeldt, J.L.: Appl. Phys. Lett. **96**, 192901 (2010)
48. Tauc, J.: Amorphous and Liquid Semiconductors. Plenum, New York (1974)